Journal of Solid State Chemistry **155,** 198–205 (2000)
doi:10.1006/jssc.2000.8934, available online at http://www.idealibrary.com on IDEAL®

Electronic Band Structure of Cadmium Chromium Chalcogenide Spinels: $CdCr_2S_4$ and $CdCr_2Se_4$

N. Shanthi, Priya Mahadevan, and D. D. Sarma[1]

Solid State and Structural Chemistry Unit, Indian Institute of Science, Bangalore 560012, India

Received June 5, 2000; in revised form August 8, 2000; accepted August 15, 2000

DEDICATED TO PROFESSOR J. M. HONIG

We report *ab initio* band structure results for two chromium chalcogenide spinels, $CdCr_2S_4$ and $CdCr_2Se_4$. Electronic structures have been calculated for both the nonmagnetic and the ferromagnetic states. The calculations correctly predict $CdCr_2Se_4$ to be a ferromagnetic insulator. The results for $CdCr_2S_4$ correspond to a ferromagnetic semimetallic ground state, with very low density of states at the Fermi energy and a nearly gapped structure. Strong exchange splitting in both compounds suggests the possibility of realizing a half-metallic ferromagnetic state in doped Cr chalcogenide spinels. © 2000 Academic Press

Key Words: **electronic band structure; chromium chalcogenide spinels; linearized muffintin orbital method.**

I. INTRODUCTION

There has been intense research activities involving ferromagnetic compounds of first-row transition metals in recent times. Much of the interest is centered around the observation of colossal negative magnetoresistive (CMR) effect due to its potential technological implications. Most of the studies are related to hole-doped manganites (1), which are ferromagnetic metals. An application of magnetic field close to T_c in these perovskite systems suppresses the resistivity drastically, giving rise to the CMR. More recently, a double perovskite without any manganese, Sr_2FeMoO_6, has also been reported (2–4) to have CMR properties. CMR behavior in these compounds are closely related to the double-exchange mechanism (5, 6). Most interestingly, $FeCr_2S_4$, which is also reported to have substantial negative magnetoresistance (7), forms in the spinel structure and contains no manganese ion. In view of this, magnetic chalcogenide spinels are becoming an interesting class of compounds in terms of their electronic and magnetic properties. In this report, we investigate the electronic and magnetic structures of two such chalcogenide spinels, $CdCr_2S_4$ and $CdCr_2Se_4$, using *ab initio* band structure calculations.

Chromium chalcogenide spinels $CdCr_2S_4$ and $CdCr_2Se_4$ are ferromagnetic semiconductors (8), with the ferromagnetic transition temperatures (9) being 84.5 K for $CdCr_2S_4$ and 129.5 K for $CdCr_2Se_4$. They also exhibit negative magnetoresistance, with $\sim 4\%$ increase in conductivity with the application of a 7-kG magnetic field in the case of $CdCr_2S_4$. Both compounds are found to show a negative temperature coefficient of resistivity in the para- and ferromagnetic regions without any discontinuity at the Curie temperature. Other ferromagnetic semiconductors, such as $HgCr_2Se_4$, are also found to exhibit a large negative magnetoresistance, due to the reduction of spin disorder upon application of a magnetic field (10). A related compound, $CuCr_2S_4$, has recently been shown to be half-metallic, while $FeCr_2S_4$ and $Fe_{0.5}Cu_{0.5}Cr_2S_4$ are found to be insulating (11). Earlier band structure calculations on these systems employed the extended Hückel empirical method (12) and self-consistent $X\alpha$ calculations (13). These approaches suffer from the limitation of being semiempirical; consequently, the previously reported band structures are substantially different from what we have obtained from the present *ab initio* calculations. For example, the width of the *d* bands turns out to be much larger (of the order of 2–3 eV) in our calculations, compared to the earlier results. Goodenough has provided phenomenological energy diagrams for a number of thiospinels and discussed the various energetics (14). More recently, $CdCr_2Se_4$ has been studied using the full-potential linearized augmented plane wave (FPLAPW) method by Continenza *et al.* (15). The density of states obtained in Ref. 15 is very similar to what we have obtained. However, there has been no report of a detailed analysis of the bonding in terms of a COHP analysis or tight-binding parametrization of the electronic structure of $CdCr_2Se_4$. We present results of such analysis here and report a comparative study between $CdCr_2S_4$ and $CdCr_2Se_4$.

We present, in this paper, the electronic band structure calculations for $CdCr_2S_4$ and $CdCr_2Se_4$, within the local

[1] To whom correspondence should be addressed. Also at the Jawaharlal Nehru Centre for Advanced Scientific Research, Bangalore. Fax: 91- 80-3601310. E-mail: sarma@sscu.iisc.ernet.in.

0022-4596/00 $35.00

spin-density approximation, using the linearized muffin-tin orbital method in the atomic-sphere-approximation (LMTO-ASA) (16). We have also performed the nonmagnetic calculations for both these compounds to investigate the bonding and the underlying basic electronic structure. We analyze the band dispersions for the nonmagnetic case in terms of a nearest-neighbor tight-binding model to extract the hopping interaction strengths (17, 18). We discuss the insulating nature of the ferromagnetic $CdCr_2S_4$ and $CdCr_2Se_4$ and also present the estimates for the exchange parameter, J.

II. DETAILS OF CALCULATIONS

We have used the LMTO-ASA method to calculate the band structure of $CdCr_2S_4$ and $CdCr_2Se_4$. Both the compounds form in the spinel structure AB_2X_4, where the anions X are arranged in a cubic close-packed lattice, with the A cations in the tetrahedral and the B cations in the octahedral sites (19), shown schematically in Fig. 1. In the figure, we have only shown some of the tetrahedral and octahedral motifs for the sake of clarity. The tetrahedral motifs are connected to neighboring octahedral motifs through corner-sharing ligand sites, while neighboring-octahedra are connected by edge-sharing. $CdCr_2S_4$ has a lattice constant $a = 10.207$ Å, with the fractional atomic coordinate, u parameter, for the S atoms being 0.375 (12). $CdCr_2Se_4$ similarly forms in the cubic spinel structure with the lattice constant $a = 10.721$ Å and $u = 0.383$ for the Se atom positions (12). There are two formula units per unit cell; 16 empty spheres, with two different symmetries, denoted E and E1, were required to satisfy the "volume-filling" criterion of ASA with overlaps between atomic spheres being less than 16%. Sphere radii used in the case of $CdCr_2S_4$ were 1.303 Å for Cd, 1.7 Å for Cr, 1.259 Å for S, 1.29 Å for E, and 1.072 Å for E1, respectively. Self-consistency was achieved using s, p, and d partial waves as the basis for Cd and Cr, s and p components for S, and only s functions in the case of the empty spheres. There were 4 empty spheres of the type E and 12 of E1 type. Self-consistency was achieved with 47 k points in the irreducible part of the Brillouin zone. Similarly, in the case of $CdCr_2Se_4$, once again 16 empty spheres were required to fill the unit cell volume with reasonable overlaps of atomic spheres and 47 irreducible k points were used for the self-consistency. Sphere radii used for Cd, Cr, Se, E, and E1 were 1.411, 1.558, 1.428, 1.257, and 1.215 Å, respectively, in the case of $CdCr_2Se_4$. In addition to the regular band structure calculations, we have also evaluated the crystal orbital Hamilton population (COHP) to understand the chemical bonding. COHP is the density of states weighted by the corresponding Hamiltonian matrix elements, which if positive indicates a bonding character and when negative indicates an antibonding character. To understand the role of magnetic interactions in these compounds, we have performed the band structure calculations for both the nonmagnetic and magnetic states of the compounds, using spin-restricted and spin-polarized calculations. This has enabled us to discuss the electronic structure of the nonmagnetic compounds in terms of the basic crystal-field effects due to the constituent CrX_6 (X = S or Se) octahedra, which play a major role in determining the underlying electronic structure. A comparison of these results with those obtained from spin-polarized calculations for the ferromagnetic ground state leads to a better understanding of the electronic structure of these magnetic spinels.

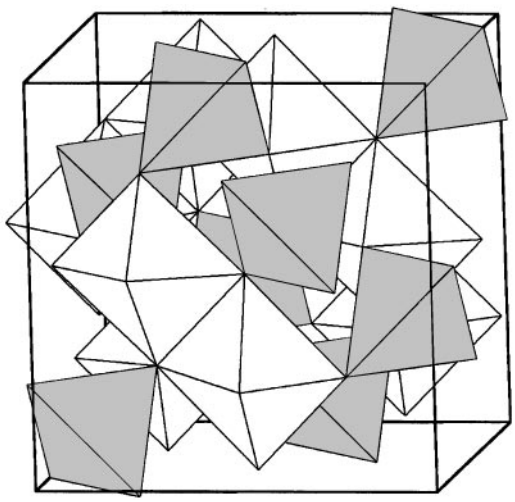

FIG. 1. A schematic representation of the spinel structure of $CdCr_2X_4$ (X = S or Se). X atoms occupy the corners of the octahedra and tetrahedra; Cd and Cr are at the centers of the tetrahedra and octahedra, respectively.

III. RESULTS AND DISCUSSION

In Fig. 2a we show the density of states (DOS) of $CdCr_2S_4$, along with the partial densities of states of Cr d and S p characters. LMTO-ASA calculations of the nonmagnetic $CdCr_2S_4$ yields a metallic state with a finite density of states at the Fermi level. The total DOS is almost entirely made up of Cr d and S p partial DOS, arising from the CrS_6 octahedra. The DOS features can be grouped roughly into three regions marked A, B, and C shown in Fig. 2a. The feature A has larger contributions from S p states with a substantial admixture of Cr d states, while the features B and C primarily originate from the Cr d bands. Thus, the DOS feature A is the Cr d–S p bonding states, with features B and C arising from the antibonding Cr d–S p interactions. The antibonding states are clearly separated into two groups (B and C) due to the octahedral crystal field of the CrS_6 units into t_{2g}^* (B) and e_g^* (C) bands. The Cr t_{2g} levels interact with the S p levels via the $pd\pi$ interactions, while the e_g bands interact via the $pd\sigma$

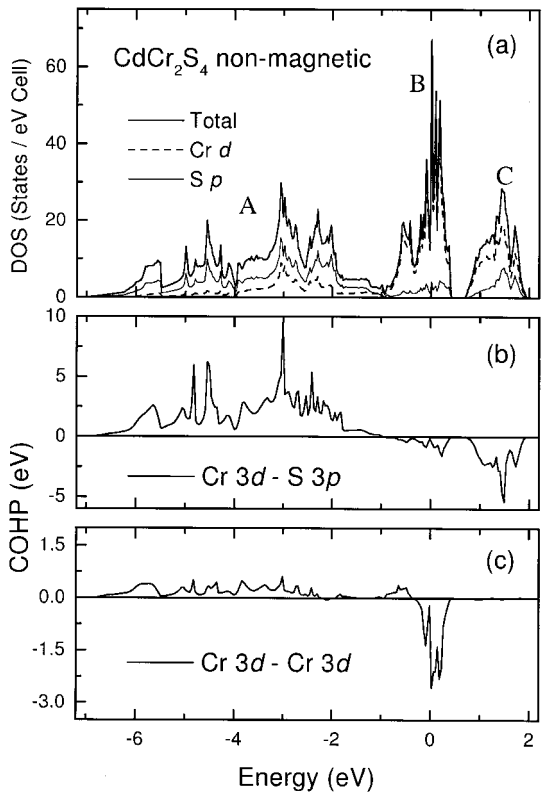

FIG. 2. (a) Density of states/eV cell of nonmagnetic $CdCr_2S_4$. Solid line is the total DOS. Dashed line is the Cr *d* partial DOS and dotted line the S *p* partial DOS. (b) COHP of Cr 3*d*–S 3*p* interaction. (c) COHP of Cr 3*d*–Cr 3*d* interaction.

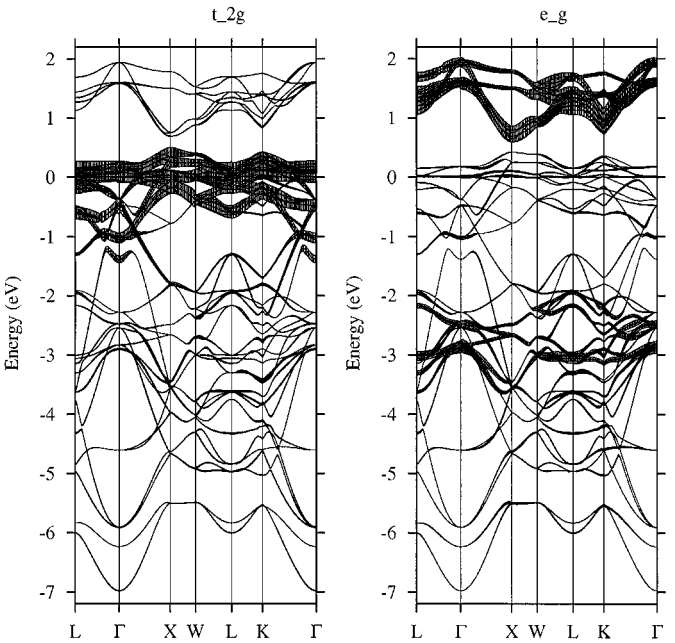

FIG. 3. The left panel shows band dispersions of nonmagnetic $CdCr_2S_4$, with Cr t_{2g} contributions shown as fat bands. The right panel shows the same dispersions, but with e_g contributions shown as fat bands.

interactions. We show the COHP of Cr 3*d*–S 3*p* interactions in Fig. 2b and Cr 3*d*–Cr 3*d* in Fig. 2c. Both of them show a positive COHP in the energy region of the feature marked A and negative in the energy regions marked B and C, confirming the above-mentioned interpretations of the various DOS features. Apart from a major contribution from Cr 3*d*–S 3*p* interactions, we find that direct Cr *d*–Cr *d* interactions contribute significantly in the energy range, where the dominant contribution is from the t_{2g} orbital.

The band dispersions along various symmetry directions are shown in Fig. 3 in terms of fat bands (20). While both panels in Fig. 3 show the same dispersions, the "fatness" of the individual band dispersions in the left panel are proportional to the Cr t_{2g} contributions, while that in the right panel is given by the Cr e_g contributions. From these figures, it is clear that the 12 bands between approximately -1.5 and 0.5 eV have primarily Cr t_{2g} characters; these 12 bands arise from the four Cr atoms in the unit cell, each contributing three spin-degenerate orbitals, namely, d_{xy}, d_{yz}, and d_{zx}. These 12 bands, with their comparatively small dispersions, are responsible for the structured DOS feature marked B in Fig. 2. Since Cr^{3+} ions have a d^3 electronic configuration, the t_{2g} band is half-filled in the nonmagnetic case, leading to the Fermi energy, E_F, being in the middle of the t_{2g} DOS. There are 8 bands between approximately 0.5 and 2 eV with evidently Cr e_g character (see Fig. 3, right panel). These arise primarily from the $d_{x^2-y^2}$ and $d_{3z^2-r^2}$ orbitals of Cr with an antibonding combination with S *p* orbitals of the same symmetry. These e_g^* bands are responsible for the Cr *d* dominated DOS feature marked C in Fig. 2a, appearing above E_F. The e_g^* bands are found to have larger dispersions than the t_{2g}^* bands, due to the fact that the $pd\sigma$ interaction strength dominating Cr e_g–S *p* interactions is larger than the $pd\pi$ interaction controlling Cr t_{2g} – S *p* interactions. There are 24 bands in the energy range of -1.0 to -7.0 eV, arising from the three *p* orbitals contributed by each of the 8 sulfur atoms in the unit cell interacting with the Cr *d* states.

To obtain a more quantitative description of the electronic structure of this compound, we have analyzed the *ab initio* band dispersions in terms of a tight binding model, details of which can be found in our earlier publications (17, 18). The essential aspects of the tight binding calculation are the inclusion of only Cr *d* and S *p* orbitals in the real crystal structure. The hopping interactions are parametrized in terms of Slater–Koster integrals (21), which are varied to obtain the best fit to the band dispersions calculated within the LMTO-ASA method. While our earlier investigations of perovskite oxides suggested that only metal *d*–ligand *p* interactions along with ligand *p*–ligand *p* hoppings are sufficient to provide a realistic description of the band dispersions, in the present case the *ab initio* bands could not be fitted with only these interactions. We additionally re-

quired Cr d–Cr d hopping interactions in the model; in the spinel structure, the Cr–Cr distance is the same as the S–S distance, unlike that in the perovskite structure. Various hopping interactions obtained from this tight binding analysis are $pd\sigma = -0.89$, $pd\pi = 0.43$, $pp\sigma = 0.5$, $pp\pi = -0.27$, $dd\sigma = -0.19$, $dd\pi = 0.12$, and $dd\delta = -0.2$ eV. It is to be noted that $pd\sigma$ is about twice as large as $pd\pi$, in agreement with earlier findings (17, 18). However, we find that the $pd\sigma$ in $CdCr_2S_4$ is considerably smaller than that in $LaCrO_3$ (17, 18). This, in addition to the Cr–S–Cr bond angle being 90° in $CdCr_2S_4$, leads to a much reduced e_g^* bandwidth compared to that in $LaCrO_3$. Interestingly, the t_{2g}^* bandwidth of $CdCr_2S_4$ is comparable to that in $LaCrO_3$. This is caused by a substantial hopping interaction between the t_{2g} orbitals at the neighboring Cr sites in the spinel structure. Thus, there is a competition between the Cr–S and direct Cr–Cr interactions in these compounds in contrast to the perovskite structure. The tight binding analysis also suggests a bare crystal-field splitting of about 1.1 eV. Having discussed the essential features of the nonmagnetic $CdCr_2S_4$, we now turn to the spin-polarized calculation.

In Fig. 4, we show the total DOS along with S p partial DOS for ferromagnetic $CdCr_2S_4$ in the upper panel; the lower panel shows the Cr $d\uparrow$ and $d\downarrow$ partial DOS. While the DOS features below -1 eV remain similar to the nonmagnetic case shown in Fig. 2 with a dominance of S p states, the DOS features related primarily to Cr d states appearing above -1 eV are distinctly different compared to those in Fig. 2. In the case of the ferromagnetic $CdCr_2S_4$, there is a further splitting of the crystal-field split Cr d bands, due to the intraatomic exchange interactions (J) into t_{2g} up-spin and t_{2g} down-spin and e_g up-spin and e_g down-spin bands. It is seen from Fig. 4 that the Cr d up-spin partial DOS appears in the unoccupied part, above the Fermi level but for the small admixture in the bonding counterpart at about -2.0 eV. Of the down-spin Cr d DOS, the t_{2g} part is fully occupied and is below the Fermi level and the e_g part is above the Fermi level. This can be clearly seen from the corresponding band dispersions shown in Fig. 5 in four panels. The upper panels show the band dispersions for the up-spin states, while the lower two panels are for the down-spin states. The left two panels show t_{2g} character as fat bands, while the two right panels show the fat bands corresponding to the e_g character. Clearly, the e_g^* bands for both up and downspins appear above the E_F. t_{2g}^* up-spin bands are also found to be above E_F, while those corresponding to the down-spin t_{2g}^* are below E_F. This suggests that Cr^{3+} is in the $t_{2g\downarrow}^3\, t_{2g\uparrow}^0\, e_{g\downarrow}^0\, e_{g\downarrow}^0$ state, as is expected in the presence of strong crystal field and exchange splittings. It can be seen that t_{2g}^* up-spin and e_g^* down-spin bands overlap energetically, giving rise to the DOS feature between approximately 0 and 2 eV, while the DOS feature between 2 and 4 eV is entirely due to the e_g^* up-spin band. The occupied t_{2g}^* down-spin band appears between -1.5 and 0 eV. Thus, the total

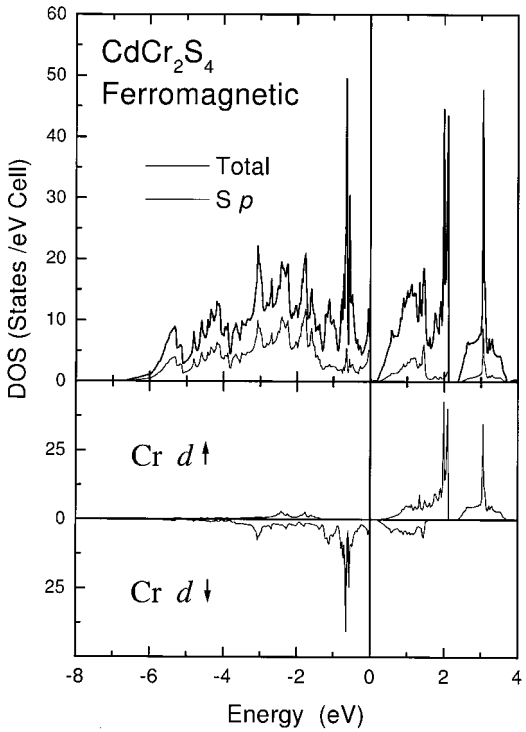

FIG. 4. Upper panel shows the DOS of ferromagnetic $CdCr_2S_4$, in terms of the total (solid line) and the S p partial (thin line) DOS. Cr d up spin of $CdCr_2S_4$ partial DOS along the positive y-axis and Cr d down-spin PDOS along the negative y-axis are shown in the lower panel.

crystal-field splitting between the up-spin t_{2g}^* and up-spin e_g^* as well as that between the down-spin counterparts is about 1.5 eV; this includes the effect of hybridization shifts. The exchange splitting between the up- and down-spin t_{2g}^* and that between the up- and down-spin e_g^* is about 2 eV. The crystal-field splitting is thus less than the exchange splitting. In these calculations, $CdCr_2S_4$ appears to be semimetallic with very low DOS at E_F, while experimentally it is known to be semiconducting. This arises from the well-known limitation of such local spin-density approximation in treating Coulomb correlations. A proper treatment of such correlation effects would lead to a narrowing of the individual band dispersions, opening up a gap at E_F. However, it is interesting to note that even the present calculation leads to an almost gapped DOS at E_F.

The basic electronic structure of $CdCr_2Se_4$ is similar to that of $CdCr_2S_4$ discussed so far. The DOS of nonmagnetic $CdCr_2Se_4$ is shown in Fig. 6a. The total DOS here is almost entirely made up of the Cr d partial DOS and Se p partial DOS, also shown in the figure. The various DOS features (A, B, and C) can be identified in a way similar to that in the case of $CdCr_2S_4$. COHP of Cr 3d–Se 4p contributions to the bonding, shown in Fig. 6b and that for the Cr 3d–Cr 3d interactions shown in Fig. 6c, also allow for similar interpretations, as in the case of $CdCr_2S_4$. This is further sup-

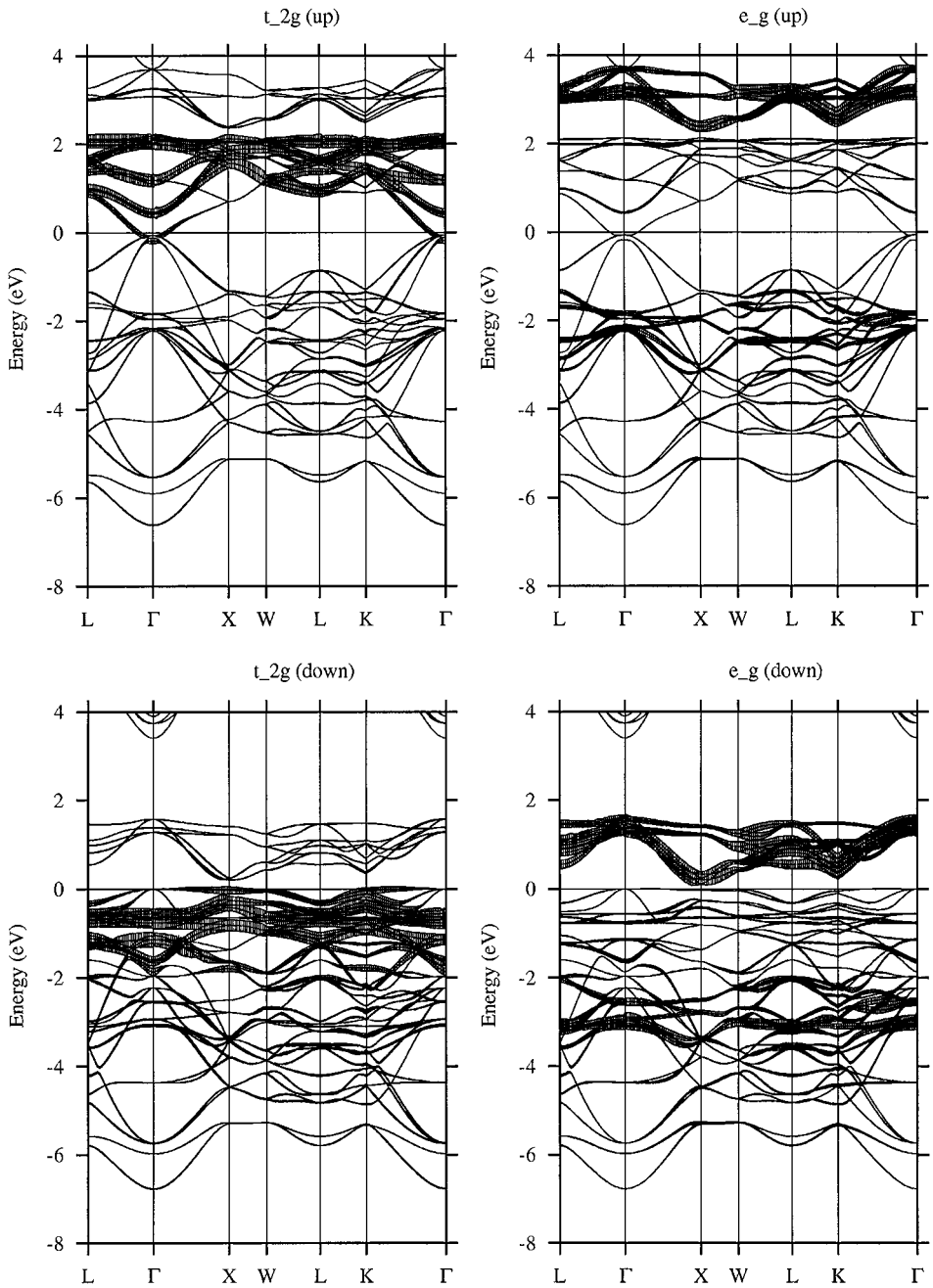

FIG. 5. Band dispersions of ferromagnetic $CdCr_2S_4$ are shown along various symmetry directions. The top two panels are for the up-spin and the bottom two for the down-spin channels. The two panels on the left show the t_{2g} contributions, while the right panels show the e_g contributions in terms of fat bands.

ported by the corresponding band dispersions shown in Fig. 7, yielding a very similar interpretation. In the case of $CdCr_2Se_4$ also, the nonmagnetic state turns out to be metallic, with the Fermi level lying in the high DOS region of the t_{2g}^* feature. As in the case of $CdCr_2S_4$, the position of E_F at the peak of a narrow DOS feature suggests a Stoner instability, indicating a magnetic ground state of the system. The DOS of nonmagnetic and also ferromagnetic $CdCr_2Se_4$ compare well with those reported in Ref. (15) obtained using the full-potential linearized augmented plane wave calculations.

Density of states of ferromagnetic $CdCr_2Se_4$ is shown in the upper panel of Fig. 8, along with the Se p partial DOS. The lower panel of Fig. 8 shows the up- and down-spin Cr d contributions. For the sake of clarity, the down-spin DOS is shown along the negative axis. Here also the up-spin

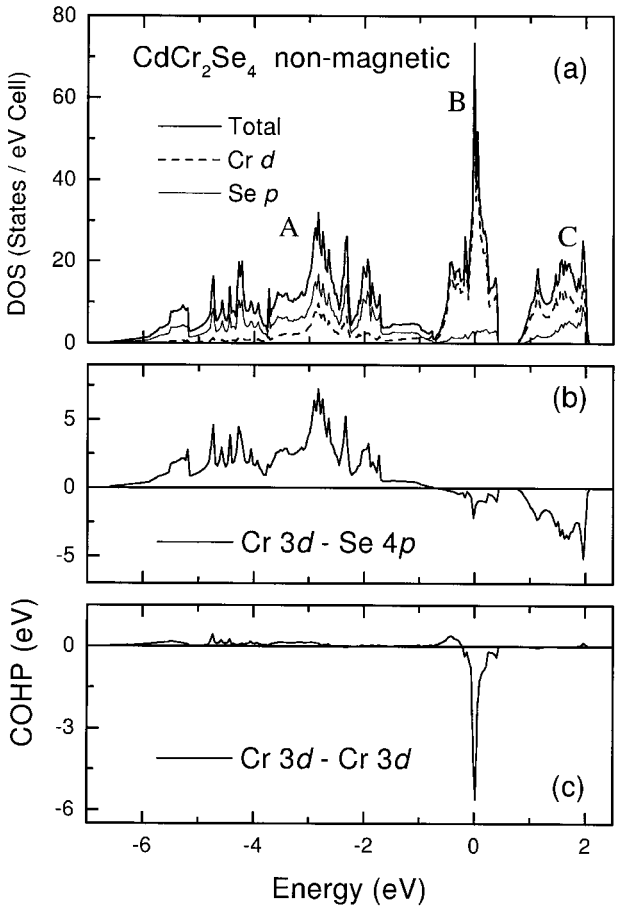

FIG. 6. (a) Density of states/eV cell of nonmagnetic $CdCr_2Se_4$. Solid line is the total DOS. Dashed line is the Cr d partial DOS and dotted line the Se p partial DOS. (b) COHP of Cr 3d–Se 4p interaction. (c) COHP of Cr 3d–Cr 3d interaction.

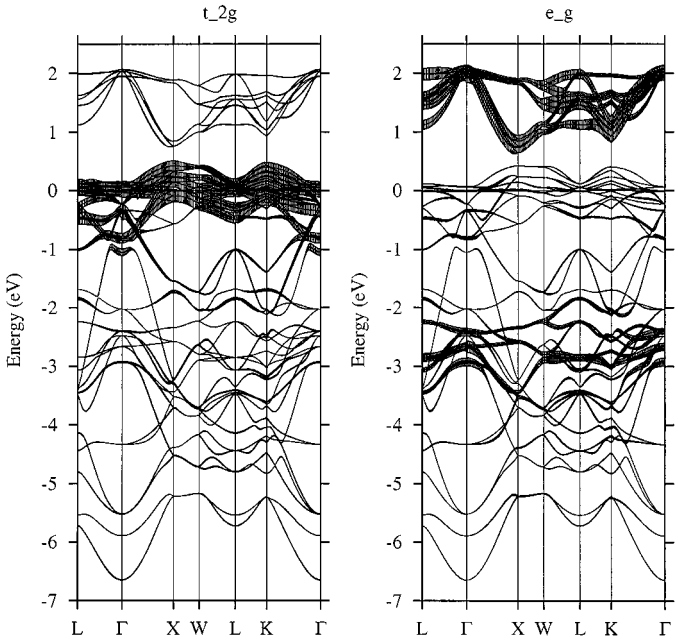

FIG. 7. The left panel shows band dispersions of nonmagnetic $CdCr_2Se_4$, with Cr t_{2g} contributions shown as fat bands. The right panel shows the same dispersions, but with e_g contributions shown as fat bands.

t_{2g}^* and up- and down-spin e_g^* bands appear above the E_F. The down-spin t_{2g}^* is completely occupied and is below E_F. The corresponding band dispersions are shown in Fig. 9 in four panels, providing the characters of each group of bands in terms of t_{2g} and e_g characters. The total crystal-field splitting in the case of $CdCr_2Se_4$ is 1.75 eV, with up-spin t_{2g}^* and e_g^* appearing at about 1.25 and 3 eV, respectively. The exchange splitting is found to be about 2.25 eV, with up-spin t_{2g}^* (e_g^*) appearing at about 1.25 eV (at 3 eV) and the down-spin t_{2g}^* (e_g^*) appearing at -1.0 eV (0.75 eV), respectively. This indicates that both crystal-field and exchange splittings are larger in $CdCr_2Se_4$ compared to those in $CdCr_2S_4$. The DOS features, particularly B and C, in $CdCr_2Se_4$ are slightly narrower than those in the case of $CdCr_2S_4$. As a result of this band narrowing, the calculated density of states exhibits a clear gap at E_F for $CdCr_2Se_4$ (see Fig. 8), in agreement with the experimentally observed semiconducting ground state of this compound. This suggests that the semiconducting ground state of chalcogenide

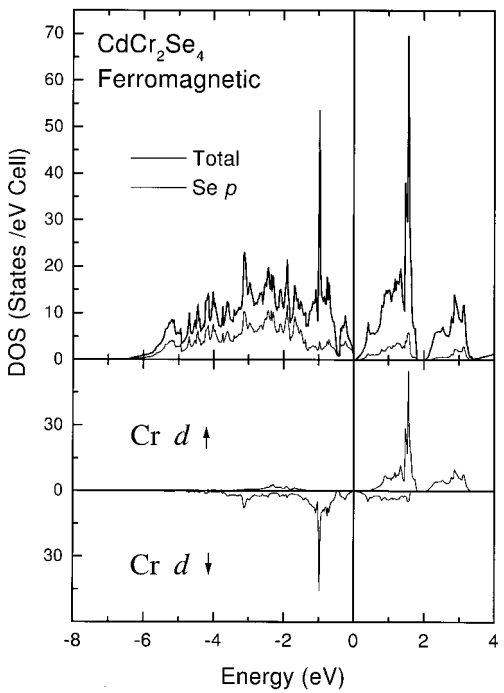

FIG. 8. Upper panel shows the DOS of ferromagnetic $CdCr_2Se_4$, in terms of the total (solid line) and the Se p partial (thin line) DOS. Cr d up spin of $CdCr_2Se_4$ partial DOS along the positive y-axis and Cr d down-spin PDOS along the negative y-axis are shown in the lower panel.

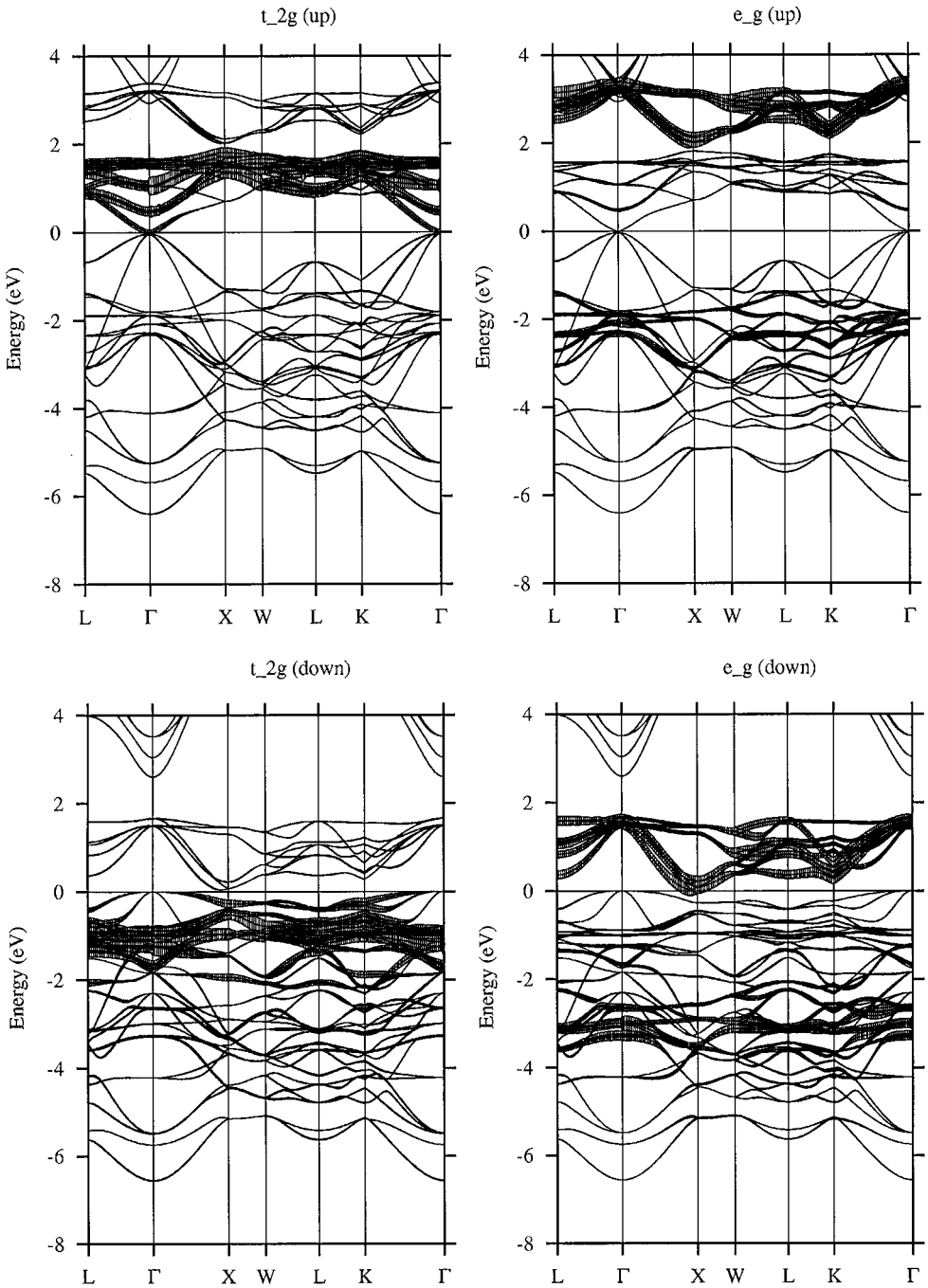

FIG. 9. Band dispersions of ferromagnetic $CdCr_2Se_4$ are shown along various symmetry directions. The top two panels are for the up-spin and the bottom two for the down-spin channels. The two panels on the left show the t_{2g} contributions, while the right panels show the e_g contributions in terms of fat bands.

spinels is primarily driven by large crystal-field and exchange splittings.

In addition to predicting the correct ground state for $CdCr_2Se_4$ and nearly correct one for $CdCr_2S_4$, it turns out that the LSDA calculated magnetic moments are also comparable to those obtained experimentally. Thus, the calculated magnetic moment of $CdCr_2S_4$ is $\sim 6.3\,\mu_B$ per formula unit, close to the experimental value of $5.7\,\mu_B$ per formula unit (22). The calculated magnetic moment of $CdCr_2Se_4$ is $\sim 6.2\,\mu_B$ per formula unit compared to the experimental value of $5.6\,\mu_B$/formula unit (9). It is interesting to note that large exchange splittings in both the compounds lead to strong polarization of the up and downspin densities of states. In particular, there is a 100% spin polar-

ization below E_F over a wide energy window in both the compounds. Even above E_F, a complete spin polarization is realized over a somewhat narrower energy window. This opens up the fascinating possibility of doping these chalcogenide spinels with nonmagnetic heterovalent impurities at the Cr sites to dope holes or electrons and realize a fully polarized half-metallic ferromagnetic state. An experimental search for such doped systems appears to be a promising task.

IV. CONCLUSION

In conclusion, we have studied the electronic band structure of ferromagnetic semiconducting spinels, $CdCr_2S_4$ and $CdCr_2Se_4$, using the scalar relativistic spin-polarized LMTO-ASA method. By carrying out the nonmagnetic calculations for both the compounds, we discussed the basic mechanisms to understand the underlying bonding and electronic structure. From spin-polarized calculations, the exchange splitting is found to be larger than the crystal-field splitting, for both the compounds. This leads to a strong spin polarization of the bands, suggesting possibilities of realizing a half-metallic ferromagnetic state in doped Cr chalcogenide spinels.

ACKNOWLEDGMENT

We thank Dr. O. K. Andersen and Dr. O. Jepsen for making the LMTO-ASA band structure program available to us.

REFERENCES

1. R. von Helmolt, J. Wocker, B. Holzaphel, M. Scholtz, and K. Samwer, *Phys. Rev. Lett.* **71,** 2331 (1993).
2. K.-I. Kobayashi, T. Kimura, H. Sawada, K. Terakura, and Y. Tokura, *Nature* **395,** 677 (1998). H. Asano, S. B. Ogale, J. Garrison, A. Orozco, Y. H. Li, E. Li, V. Smolyaninova, C. Galley, M. Downes, M. Rajeswari, R. Ramesh, and T. Venkatesan, *Appl. Phys. Lett.* **74,** 3696 (1999).
3. D. D. Sarma, E. V. Sampathkumaran, S. Ray, R. Nagarajan, S. Majumdar, A. Kumar, G. Nalini, and T. N. Guru Row, *Solid State Commun.* **114,** 465 (2000).
4. D. D. Sarma, P. Mahadevan, T. Saha-Dasgupta, S. Ray, and A. Kumar, *Phys. Rev. Lett.* **85,** 2549 (2000).
5. C. Zener, *Phys. Rev.* **82,** 403 (1951).
6. P. W. Anderson and H. Hasegawa, *Phys. Rev. B* **100,** 67 (1955).
7. A. P. Ramirez, R. J. Cava, and J. Krajewski, *Nature* **386,** 156 (1997).
8. P. K. Baltzer, H. W. Lehmann, and M. Robbins, *Phys. Rev. Lett.* **15,** 493 (1965), H. W. Lehmann and M. Robbins, *J. Appl. Phys.* **37,** 1389 (1966).
9. P. K. Baltzer, P. J. Wojtowicz, M. Robbins, and E. Lopatin, *Phys. Rev.* **151,** 367 (1966).
10. A. Selmi, P. Gibart, and L. Goldstein, *J. Magn. Magn. Mater.* **15–18,** 1285 (1980).
11. M. S. Park, S. K. Kwon, S. J. Youn, and B. I. Min, *Phys. Rev. B* **59,** 10018 (1999).
12. T. Kambara, T. Oguchi, and K. I. Gondaira, *J. Phys. C* **13,** 1493 (1980).
13. T. Oguchi, T. Kambara, and K. I. Gondaira, *Phys. Rev. B* **22,** 872 (1980).
14. J. B. Goodenough, *J. Phys. Chem. Solids* **30,** 261 (1969).
15. A. Continenza, T. de Pascale, F. Meloni, and M. Serra, *Phys. Rev. B* **49,** 2503 (1994).
16. O. K. Andersen, *Phys. Rev. B* **12,** 3060 (1975). O. K. Andersen and R. V. Kasowski, *Phys. Rev. B* **4,** 1064 (1971). O. K. Andersen, *Solid State Commun.* **13,** 133 (1973).
17. P. Mahadevan, N. Shanthi, and D. D. Sarma, *J. Phys. Condens. Matter* **9,** 3129 (1997).
18. P. Mahadevan, N. Shanthi, and D. D. Sarma, *Phys. Rev B* **54,** 11199 (1996).
19. A. R. West, "Solid State Chemistry and Its Applications." Wiley, New York, 1984.
20. O. Jepsen and O. K. Andersen, *Z. Phys. B* **97,** 35 (1995).
21. J. C. Slater and G. F. Koster, *Phys. Rev.* **94,** 1498 (1954).
22. H. L. Pinch and S. B. Berger, *J. Phys. Chem. Solids* **29,** 2091 (1968).